J. Fluid Mech. (1990), *vol.* 218, *pp.* 19–39
Printed in Great Britain

Sand ripples under sea waves
Part 2. Finite-amplitude development

By G. VITTORI AND P. BLONDEAUX
Istituto di Idraulica, Università di Genova, Via Montallagero, 1, 16145 Genova, Italy

(Received 1 December 1988 and in revised form 14 June 1989)

In the present paper we formulate a theory to predict the time development of sand ripples characterized by small but finite amplitude under the action of surface gravity waves. The theory is based on a weakly nonlinear stability analysis of a flat sandy bottom subject to viscous oscillatory flow. The parameters of the problem (namely the Reynolds number of the flow and the Reynolds and Froude numbers of sediments) are assumed to fall within a neighbourhood of the critical conditions determined in Blondeaux (1990). The analysis can predict the actual ripple height, wavelength and profile when flow separation is absent, i.e. for the case of rolling-grain ripples. Assuming Sleath's (1984) criterion for separation, the values of the relevant parameters at which transition from rolling-grain ripples to vortex ripples occurs are predicted. A comparison between theoretical findings and experimental data supports the validity of the present theory.

1. Introduction

In the companion paper (Blondeaux 1990, hereinafter referred to as I), the senior author has analysed ripple formation underneath a gravity wave by developing a linear stability analysis which allowed the determination of the threshold conditions for the growth of infinitesimal perturbations of a flat sandy bottom subject to a viscous oscillatory flow.

Results of I show that for fixed values of the Reynolds number R_δ of the bottom boundary layer and the particle Reynolds number R_d, a critical value of the particle Froude number F_d exists (F_{dc}) such that (i) for $F_d < F_{dc}$ bottom perturbations decay for each real value of the perturbation wavenumber α; (ii) for $F_d > F_{dc}$ bottom perturbations characterized by wavenumbers falling within a restricted range experience a net amplification during a cycle. (In this paper we adopt the notation and definitions of I.) The above analysis also allows the prediction of ripple wavelength at the critical conditions.

However, being based on a linear stability analysis, the above work is unable to follow the temporal development of finite-amplitude perturbations and predict whether they eventually reach a final equilibrium amplitude and its value. The latter goal is of some interest. Indeed it is well known (Sleath 1984) that for values of the ratio k between ripple height and ripple wavelength larger than about 0.1, flow separates behind the crests and vortex ripples develop. An analysis which could predict the actual ripple height and wavelength as a function of the physical parameters of the problem could then predict the value of k and consequently the actual bed configuration (rolling-grain ripples or vortex ripples).

The mechanics of ripple initiation is explained in I: a slight perturbation of the sea bottom under an oscillatory motion produces steady streaming which tends to carry

sediment from the trough towards the crest of the perturbation, thus causing its growth. The tendency of sediment to pile up near the crests is opposed by the gravity force acting down the slope. The growth of bottom perturbations is thus controlled by a balance between the above two effects. If drag prevails over gravity the perturbation starts to grow. In this paper we try to explain the mechanism by which the perturbations reduce their growth and finally reach an equilibrium configuration. It will be shown how the phenomenon of ripple development is controlled by nonlinear effects which will be seen to inhibit the indefinite growth predicted by linear theory.

In the present paper we develop a weakly nonlinear stability analysis of a flat sandy bottom subject to a viscous oscillatory flow. Since it has been experimentally observed that the average bottom development takes place on a timescale much larger than the timescale characteristic of fluid oscillations, two timescales have been introduced thus decoupling fluid from bottom development.

The flow field has then been determined using the solution for the viscous nonlinear oscillatory flow over a wavy wall due to Vittori (1989). Then the equation describing the nonlinear evolution of the fastest growing bottom perturbation is derived for values of the relevant physical parameters falling within a neighbourhood of the critical conditions for ripple formation determined in I. This amplitude equation is of Landau–Stuart type (Stuart 1971) and allows for equilibrium amplitude solutions asymptotically reached for large times. It is worth pointing out that the equilibrium amplitude of ripples is thus related to the quantity $(F_d - F_{dc})$. Moreover in the present analysis it has been assumed, according to Sleath (1984), that vortex ripples appear as soon as the value of k exceeds the threshold value 0.1. Using this assumption and analysing the amplitude equation, a critical value of F_d for vortex-ripple formation can be determined together with the geometrical configuration of rolling-grain ripples present when the flow does not separate.

In the next section we formulate the problem and describe the method of solution. In the third section we describe some results. The last section is devoted to some conclusions.

2. Theory

Under the assumptions formulated in §2 of I we analyse the time development of a periodic bottom perturbation of small but finite amplitude when the relevant physical parameters of the problem fall within a neighbourhood of the critical conditions (determined in I) for which ripples are expected to form.

For fixed values of R_δ and R_d, we consider particle Froude numbers F_d and perturbation wavenumbers α such that

$$F_d = F_{dc} + \epsilon, \quad \alpha = \alpha_c + \epsilon\alpha_1, \tag{1a, b}$$

where ϵ is a small parameter denoting the difference between the actual sediment Froude number F_d and its critical value F_{dc}, α_c is the critical wavenumber for fixed values of R_δ and R_d, while α_1 is an arbitrary parameter of order one.

Relationships (1 a, b) imply that disturbances are followed in the weakly nonlinear regime, allowing their wavenumber α to be 'slightly' perturbed with respect to the critical value α_c.

As stated in I the problem of determining the time development of a bottom perturbation is posed by the vorticity equation and the sediment continuity equation, along with a 'constitutive' relationship between sediment flow rate and

flow characteristics. Boundary conditions are also required which force the flow field in the bottom layer to match the outer irrotational motion far from the bottom and satisfy no-slip at the bottom.

From the results described in I it can be easily verified that in the neighbourhood of the critical condition defined by (1 *a*, *b*) the amplification factor which controls the average growth of an infinitesimal bottom perturbation is of order ϵ. For this reason the process is described in terms of a fast timescale t as well as of a slow timescale τ defined by (2*a*). Thus, following the lead of Stuart (1971) we employ a multiple scale technique and define a 'slow' timescale τ associated with the average growth of perturbations such that

$$\tau = \epsilon Q t, \quad \frac{\partial}{\partial t} \to \frac{\partial}{\partial t} + \epsilon Q \frac{\partial}{\partial \tau}, \tag{2a, b}$$

where, as shown in I

$$Q = \frac{a R_d^{1-b}}{2F_d(1-n)}.$$

Thus the average growth of perturbations takes place on a timescale that is much larger than that associated with fluid oscillations. Indeed typical values of Q for sand in a laminar boundary layer at the bottom of gravity waves are smaller than one and ϵ is much smaller than one since the parameters of the problem fall within a neighbourhood of the critical conditions.

Using (2) and the non-dimensional variables defined in I, the governing differential problem reads

$$\frac{2}{R_\delta}\left(\frac{\partial}{\partial t} + \epsilon Q \frac{\partial}{\partial \tau}\right)(\nabla^2\psi) + \frac{\partial\psi}{\partial y}\frac{\partial}{\partial x}(\nabla^2\psi) - \frac{\partial\psi}{\partial x}\frac{\partial}{\partial y}(\nabla^2\psi) = \frac{1}{R_\delta}(\nabla^4\psi), \tag{3}$$

$$\frac{\partial q}{\partial x} = -\frac{2F_d}{R_d}(1-n)\left(\frac{\partial}{\partial t} + \epsilon Q \frac{\partial}{\partial \tau}\right)\eta, \tag{4}$$

$$q = a\left|\frac{2}{R_d}V - \frac{\beta}{F_d^2}\frac{\partial\eta}{\partial x}\right|^b \operatorname{sgn}\left(\frac{2}{R_d}V - \frac{\beta}{F_d^2}\frac{\partial\eta}{\partial x}\right), \tag{5}$$

$$\frac{\partial\psi}{\partial y} \to \tfrac{1}{2}e^{it} + \text{c.c.}, \quad \frac{\partial\psi}{\partial x} \to 0 \quad \text{for} \quad y \to \infty, \tag{6}$$

$$\frac{\partial\psi}{\partial y} = 0, \quad \frac{\partial\psi}{\partial x} = 0 \quad \text{for} \quad y = \eta. \tag{7}$$

The relationship (5) relating sediment flow rate to flow characteristics has been proposed in I and will not be discussed further in the present contribution.

In order to derive the order of magnitude of the amplitude of the perturbation we follow the usual argument of hydrodynamic stability: nonlinearity gives rise to interactions of the fundamental with itself and with the basic flow which lead to the generation of higher harmonics. Following the above cascade process one finds that the fundamental is reproduced at third order and secular terms are generated. In order to prevent their occurrence the 'slow' time dependence of the amplitude $\mathscr{A}$ of the fundamental must also be forced to produce a contribution at third order. In

other words $\epsilon(\partial\mathscr{A}/\partial\tau)$ must balance $\mathscr{A}^3$, which occurs provided $O(\mathscr{A}) = O(\epsilon^{\frac{1}{2}})$. We then expand the solution in the form

$$\eta(x,t,\tau) = \epsilon^{\frac{1}{2}}[A(\tau)\,C_1(t)\,\mathrm{e}^{\mathrm{i}\alpha x} + \text{c.c.}] + \epsilon[A^2(\tau)\,C_{22}(t)\,\mathrm{e}^{2\mathrm{i}\alpha x} + \text{c.c.}] + \epsilon^{\frac{3}{2}}[A^2(\tau)\,\bar{A}(\tau)\,C_{31}(t)\,\mathrm{e}^{\mathrm{i}\alpha x} + \text{c.c.}] + O(\epsilon^{\frac{3}{2}}\mathrm{e}^{3\mathrm{i}\alpha x}), \quad (8)$$

$$\begin{aligned}\psi(x,y,t,\tau) = {} & \psi_0(y,t) + \epsilon^{\frac{1}{2}}[A(\tau)\,C_1(t)\,\Phi_1(y,t)\,\mathrm{e}^{\mathrm{i}\alpha x} + \text{c.c.}] \\ & + \epsilon[A(\tau)\,\bar{A}(\tau)\,C_1(t)\,\bar{C}_1(t)\,\Phi_{20}(y,t) \\ & + A^2(\tau)\,(C_1^2(t)\,\Phi_{22}^{(1)}(y,t) + C_{22}(t)\,\Phi_{22}^{(2)}(y,t))\,\mathrm{e}^{2\mathrm{i}\alpha x} + \text{c.c.}] \\ & + \epsilon^{\frac{3}{2}}[A^2(\tau)\,\bar{A}(\tau)\,(C_1^2(t)\,\bar{C}_1(t)\,\Phi_{31}^{(1)}(y,t) + C_{31}(t)\,\Phi_{31}^{(2)}(y,t))\,\mathrm{e}^{\mathrm{i}\alpha x} + \text{c.c.}] \\ & + O(\epsilon^{\frac{3}{2}}\mathrm{e}^{3\mathrm{i}\alpha x}),\end{aligned} \quad (9)$$

where $A(\tau)$ represents the amplitude of the fundamental (averaged on a cycle) which evolves on the slow timescale τ. Notice that an overbar (or c.c.) denotes, the complex conjugate of a complex number.

In the expansion (9) for the stream function ψ various contributions appear:

(i) the stream function ψ_0 of the basic Stokes flow;

(ii) a contribution of order $\epsilon^{\frac{1}{2}}$ ($\epsilon^{\frac{1}{2}}AC_1\,\Phi_1\,\mathrm{e}^{\mathrm{i}\alpha x}$) which is forced by the fundamental bottom perturbation ($\epsilon^{\frac{1}{2}}AC_1\,\mathrm{e}^{\mathrm{i}\alpha x}$);

(iii) a contribution of order ϵ which is the sum of three terms: $\epsilon A\bar{A}C_1\,\bar{C}_1\,\Phi_{20}$, $\epsilon A^2C_1^2\,\Phi_{22}^{(1)}\,\mathrm{e}^{2\mathrm{i}\alpha x}$ and $\epsilon A^2C_{22}\,\Phi_{22}^{(2)}\,\mathrm{e}^{2\mathrm{i}\alpha x}$. The first two terms are generated by the nonlinear interaction of the flow-field component at the previous order. Since the latter is periodic along the x-direction with wavenumber α, one term is independent of x and the other is periodic with wavenumber 2α. The steady streaming associated with this fluid motion would tend to carry sediment along the bed profile thus causing the appearance of a bottom waviness with a wavelength equal to half of the fundamental ($\epsilon A^2C_{22}\,\mathrm{e}^{2\mathrm{i}\alpha x}$). This new perturbation of the bottom profile produces a further component of the stream function, namely $\epsilon A^2C_{22}\,\Phi_{22}^{(2)}\,\mathrm{e}^{2\mathrm{i}\alpha x}$;

(iv) two contributions of order $\epsilon^{\frac{3}{2}}$ proportional to $\mathrm{e}^{\mathrm{i}\alpha x}$ and to $\mathrm{e}^{3\mathrm{i}\alpha x}$ respectively. They are generated either by nonlinear effects or by the presence of a bottom perturbation of order $\epsilon^{\frac{3}{2}}$. In (8) and (9) only the term proportional to $\mathrm{e}^{\mathrm{i}\alpha x}$ is explicitly shown since the other term is not relevant to the present analysis.

Derivation of the equations for the unknown functions appearing in (8) and (9) is tedious but straightforward. The equations are obtained by substituting (8), (9) into (3)–(7) and equating like powers of ϵ. Since this is a well-established procedure and since the intermediate and resultant equations are lengthy, details are omitted. Readers not familiar with this procedure are referred to Vittori (1990).

2.1. $O(\epsilon^0)$

At $O(\epsilon^0)$ we obtain the Stokes problem. The flow field is described by the stream function $\psi_0(y,t)$ given by (22), (24) of I and sediment moves to and fro.

2.2. $O(\epsilon^{\frac{1}{2}})$

At order $\epsilon^{\frac{1}{2}}$ a problem identical to that posed by (15)–(18) of I is obtained. In order to determine the flow field a different method of solution with respect to that used in I is employed here which has the advantage of also being suitable for obtaining the solution of the differential systems obtained at higher orders. Details of the method can be found in Vittori (1989). However, it is worth summarizing here the main features of the procedure.

As in I the new coordinate system $(\tilde{x}, \tilde{y})$, which oscillates with the fluid far from the bottom, is introduced and the modified stream function $\tilde{\psi}$ is defined (see (19) and (21) of I). The latter is developed in power series in $\epsilon^{\frac{1}{2}}$:

$$\tilde{\psi} = \tilde{\psi}_0 + \epsilon^{\frac{1}{2}}[A(\tau)\, C_1(t)\, \tilde{\Phi}_1(\tilde{y}, t)\, \mathrm{e}^{\mathrm{i}\alpha\tilde{x}} + \text{c.c.}] + O(\epsilon). \tag{10}$$

Comparing (10) with (9) it follows that

$$\tilde{\Phi}_1 = \Phi_1 P(t). \tag{11}$$

The functions $\tilde{\Phi}_1$ and $P(t)$, being periodic in time, are expanded in Fourier series as in I:

$$P(t) = \sum_{m=-\infty}^{+\infty} p_m \mathrm{e}^{\mathrm{i}mt}, \quad \tilde{\Phi}_1(\tilde{y}, t) = \sum_{m=-\infty}^{+\infty} G_m(\tilde{y})\, \mathrm{e}^{\mathrm{i}mt}. \tag{12a, b}$$

Substitution of (10)–(12) into the problem at order $\epsilon^{\frac{1}{2}}$, along with (19) and (21) of I, leads to the following system of coupled ordinary differential equations for G_m:

$$\frac{2}{R_\delta}\mathrm{i}m\mathrm{N}^2 G_m + \mathrm{i}\alpha_\mathrm{c}\left[\frac{\mathrm{d}F_0}{\mathrm{d}\tilde{y}}\mathrm{N}^2 G_{m-1} + \frac{\mathrm{d}\bar{F}_0}{\mathrm{d}\tilde{y}}\mathrm{N}^2 G_{m+1}\right] - \mathrm{i}\alpha_\mathrm{c}\left[\frac{\mathrm{d}^3 F_0}{\mathrm{d}\tilde{y}^3} G_{m-1} + \frac{\mathrm{d}^3 \bar{F}_0}{\mathrm{d}\tilde{y}^3} G_{m+1}\right] = \frac{1}{R_\delta}\mathrm{N}^4 G_m, \tag{13}$$

with the following boundary conditions:

$$\frac{\mathrm{d}G_m}{\mathrm{d}\tilde{y}} + \left[\frac{\mathrm{d}^2 F_0}{\mathrm{d}\tilde{y}^2} p_{m-1} + \frac{\mathrm{d}^2 \bar{F}_0}{\mathrm{d}\tilde{y}^2} p_{m+1}\right] = G_m = 0, \quad y = 0 \tag{14a}$$

$$\frac{\mathrm{d}G_m}{\mathrm{d}\tilde{y}} \to 0, \quad G_m \to 0, \quad \tilde{y} \to \infty. \tag{14b}$$

The operator N^2 is defined as follows:

$$\mathrm{N}^2 \equiv \left(\frac{\mathrm{d}^2}{\mathrm{d}\tilde{y}^2} - \alpha_\mathrm{c}^2\right). \tag{15}$$

In (13) and (14*a*) the function F_0 coincides with that given by (24) of I. Neglecting harmonics higher than the Mth in the Fourier series (12), the functions G_m are determined numerically using a Runge–Kutta method of fourth order and a shooting procedure from infinity to ensure numerical accuracy.

More precisely: first equation (13) is solved in a closed form for large values of $\tilde{y}$ where F_0 tends to vanish and the solution behaves as follows:

$$G_m^* = a_m \mathrm{e}^{-\alpha\tilde{y}} + b_m \exp\left[-(\alpha_\mathrm{c} + 2\mathrm{i}m\tilde{y})^{\frac{1}{2}}\right]. \tag{16}$$

Notice that in (16) exponentially growing components have been dropped because of (14*b*). Secondly, starting from large values of $\tilde{y}$ ($\tilde{y}_\infty$), where G_m and its derivatives are known from (16), a set of $2M+1$ linearly independent numerical solutions $G_m^{(j)}$ are obtained assuming linearly independent values for a_m and b_m (the integration procedure makes use of a standard Runge–Kutta method of fourth order). Finally, the solution is then determined as a linear combination of $G_m^{(j)}$ which satisfies the boundary conditions (14*a*) at the wall.

The values of the starting point $\tilde{y}_\infty$ and of the number M of harmonics retained in (12*a*, *b*) have been chosen according to the following criteria. The value of $\tilde{y}_\infty$ must be large enough for the convective term in (13) to be negligible with respect to the

remaining terms of the vorticity equation. Since F_0 decreases exponentially with the distance from the wall, values of $\tilde{y}_\infty$ larger than 7 are sufficient to ensure a relative error of less than 10^{-3} for αR_δ of order one. The value of M has been chosen on the basis of numerical experiments in such a way that the contribution of the harmonics $M+1$ and $-M-1$ to the solution are negligible. The value of M depends on α and R_δ. In the range of the parameters so far investigated a maximum value $M = 25$ has been employed.

Once the stream function at order $\epsilon^{\frac{1}{2}}$ is known, the sediment continuity equation can be solved to obtain the function $C_1(t)$. Since, as stated I, the values of Q are smaller than one, $C_1(t)$ can be expanded in power series of Q in the form

$$C_1(t) = 1 + QC_1^{(1)}(t) + O(Q^2). \tag{17}$$

After substitution of (8), (9) and (17) into the sediment continuity equation and the use of the sediment flow rate formula, at order $\epsilon^{\frac{1}{2}}Q$ one finds

$$\frac{\mathrm{d}C_1^{(1)}(t)}{\mathrm{d}t} = -\mathrm{i}\alpha_c\, e(t), \tag{18}$$

where
$$e(t) = b\left|2\frac{\partial \psi_0}{\partial y}\right|^{b-1}\left[2\left(\frac{\partial^2 \psi_0}{\partial y^2}+\frac{\partial \Phi_1}{\partial y}\right)-\mathrm{i}\alpha_c\frac{\beta R_d}{F_{dc}^2}\right] \quad \text{at} \quad y = \frac{R_d}{2R_\delta}. \tag{19}$$

The solution of (18) is straightforward and leads to the following form for $C_1^{(1)}(t)$:

$$C_1^{(1)}(t) = -\mathrm{i}\alpha_c \int_{t_0}^{t} e(t)\,\mathrm{d}t. \tag{20}$$

Since $e(t)$ is a periodic function of time (indeed all functions appearing in its definition are periodic) the boundedness of $C_1^{(1)}(t)$ is ensured by the fact that the integrand which appears in (20) has a vanishing time average over a cycle. The latter conclusion is based on the observation that the physical parameters of the problem fall within a neighbourhood of the critical conditions (compare (19) with (33) of I). From a physical point of view this means that the destabilizing effects due to fluid motion which tends to carry sediment from the troughs to the crests (first two terms appearing in (19)) are exactly balanced by the effect of the component along the bed profile of the weight of the sediment (third term appearing in (19)).

2.3. $O(\epsilon)$

At order ϵ, the interaction of the leading-order perturbation with itself in the vorticity equation produces two terms in the stream function: a distortion of the basic flow (independent of the x-coordinate) and a periodic contribution with wavelength equal to half that of the fundamental. These two terms are respectively $A\bar{A}C_1\bar{C}_1\Phi_{20}$ and $A^2C_1^2\Phi_{22}^{(1)}\mathrm{e}^{2\mathrm{i}\alpha x}$. As previously explained, the steady streaming at this order of approximation tends to carry sediment along the bed profile thus causing the appearance of a bottom waviness with wavelength equal to half that of the fundamental ($A^2C_{22}\mathrm{e}^{2\mathrm{i}\alpha x}$). This new perturbation of the bottom profile produces a further component of the stream function ($A^2C_{22}\Phi_{22}^{(2)}\mathrm{e}^{2\mathrm{i}\alpha x}$) which is proportional to the amplitude A^2C_{22} of the second harmonic of the bottom. Substitution of (9) in (3), (6), (7) gives rise at order ϵ to the problems for Φ_{20}, $\Phi_{22}^{(1)}$ and $\Phi_{22}^{(2)}$ which are reported in Appendix A. The procedure followed to obtain the flow field at this order of approximation is similar to that used in §2.2 and will not be described here. Details can be found in Vittori (1989).

Once the flow is known, the sediment continuity equation is considered. As before we develop C_{22} as

$$C_{22}(t) = C_{22}^{(0)} + QC_{22}^{(1)}(t) + O(Q^2). \tag{21}$$

Substituting (8), (9) and (21) into (4) and using (5), at order ϵQ we find

$$\frac{\mathrm{d}C_{22}^{(1)}(t)}{\mathrm{d}t} = -2\mathrm{i}\alpha_c[f(t) + C_{22}^{(0)}\, g(t)], \tag{22}$$

where the functions $f(t)$ and $g(t)$ are given in Appendix B.

The time derivative of $C_{22}^{(1)}$ is thus given by the sum of two contributions. The first contribution ($-2\mathrm{i}\alpha_c f(t)$) is related to the action of the flow field arising from the nonlinearity of the vorticity equation. The second contribution ($-2\mathrm{i}\alpha_c C_{22}^{(0)} g(t)$) is simply related to the flow induced by the second harmonic of the bottom profile. It is easy to see that both $f(t)$ and $g(t)$ are periodic functions of time. So if we require that $C_{22}^{(1)}$ remains bounded, the time average over a period of the right-hand side of (22) must vanish. This condition determines the value of the constant $C_{22}^{(0)}$, i.e. the amplitude of the bottom second harmonic

$$C_{22}^{(0)} = -\frac{\int_0^{2\pi} f(t)\,\mathrm{d}t}{\int_0^{2\pi} g(t)\,\mathrm{d}t}. \tag{23}$$

From a physical point of view relationship (23) forces the amplitude of the bottom second harmonic in such a way that the gravity component along the bed profile at second order exactly balances the second-order component of the drag force acting on the sediment caused by the steady streaming associated with both $\Phi_{22}^{(1)}$ and $\Phi_{22}^{(2)}$. Then from (22) and using (23) we find

$$C_{22}^{(1)}(t) = \int_{t_0}^{t} -2\mathrm{i}\alpha_c[f(t) + C_{22}^{(0)}\, g(t)]\,\mathrm{d}t. \tag{24}$$

From what has previously been said it follows that $C_{22}^{(1)}$ is a periodic function of time.

2.4 $O(\epsilon^{\frac{3}{2}})$

The stream function at order $\epsilon^{\frac{3}{2}}$ can be split into two components: one proportional to $\mathrm{e}^{\mathrm{i}\alpha x}$ and the other to $\mathrm{e}^{3\mathrm{i}\alpha x}$. The former ($A^2\bar{A}C_1^2\Phi_{31}^{(1)}\mathrm{e}^{\mathrm{i}\alpha x}$) arises from the nonlinearity of vorticity equation and the other ($A^2\bar{A}C_{31}\Phi_{31}^{(2)}\mathrm{e}^{\mathrm{i}\alpha x}$) is forced by the presence of a bottom perturbation at order $\epsilon^{\frac{3}{2}}$. Substitution of (9) into (3), (6) and (7) generates differential problems at order $\epsilon^{\frac{3}{2}}$ for the functions $\Phi_{31}^{(1)}$ and $\Phi_{31}^{(2)}$. It is easy to verify that both problems are similar to that found for Φ_1 but for the presence of a forcing term. They are solved using the same procedure as described in §2.2.

Let us finally come to sediment continuity at $O(\epsilon^{\frac{3}{2}})$. As previously, let us expand the amplitude $C_{31}(t)$ in power series in Q of the form:

$$C_{31}(t) = C_{31}^{(0)} + QC_{31}^{(1)}(t) + O(Q^2). \tag{25}$$

Substituting (8), (9) and (25) into the sediment continuity equation and making use of the sediment flow rate formula, at order $\epsilon^{\frac{3}{2}}$ we find

$$A^2\bar{A}\frac{\mathrm{d}C_{31}^{(1)}(t)}{\mathrm{d}t} = -\frac{\partial A}{\partial \tau} - A^2\bar{A}\mathrm{i}\alpha_c\, l(t)$$

$$-A\left[\left(\mathrm{i}\alpha_1 - \frac{\mathrm{i}\alpha_c c}{F_{dc}}\right)h(t) - \mathrm{i}\alpha_c b\left|2\frac{\partial \psi_0}{\partial y}\right|^{b-1}\left(\mathrm{i}\alpha_1\frac{\beta R_d}{F_{dc}^2} - 2\mathrm{i}\alpha_c\frac{\beta R_d}{F_{dc}^3}\right)\right] \quad \text{at} \quad y = \frac{R_d}{2R_\delta}$$

$$+\text{terms proportional to } C_{31}^{(0)}\, e(t), \tag{26}$$

where the constant c is equal to 2.83, the functions $h(t)$, $l(t)$ are given in Appendix C and $e(t)$ is defined by (19).

Again in order to avoid secular terms in the solution of (26), the time average over a cycle of the right-hand side of (26) must vanish. The time average of the term proportional to $C_{31}^{(0)}$ is zero for any value of $C_{31}^{(0)}$ since the values of the physical parameters fall within a neighbourhood of the critical conditions. By imposing that the time average over a cycle of the remaining part of (26) should vanish, the following ordinary differential equation for $A(\tau)$ is obtained:

$$\frac{\mathrm{d}A(\tau)}{\mathrm{d}\tau} = a_1 A(\tau) + a_2 A^2(\tau)\bar{A}(\tau), \tag{27}$$

where a_1, a_2, are functions of the relevant physical parameters:

$$a_1 = -\int_0^{2\pi}\left[\left(\mathrm{i}\alpha_1 - \frac{\mathrm{i}\alpha_c c}{F_{dc}}\right)h(t) - \mathrm{i}\alpha_c b\left|2\frac{\partial \psi_0}{\partial y}\right|^{b-1}\left(\mathrm{i}\alpha_1\frac{\beta R_d}{F_{dc}^2} - 2\mathrm{i}\alpha_c\frac{\beta R_d}{F_{dc}^3}\right)\right]\mathrm{d}t, \tag{28a}$$

$$a_2 = -\int_0^{2\pi}\mathrm{i}\alpha_c\, l(t)\,\mathrm{d}t. \tag{28b}$$

Equation (27) is of Landau–Stuart type and can be easily integrated in closed form to obtain the time development of a small initial bottom perturbation and its asymptotic behaviour for large time:

$$|A(\tau)| = \left[\frac{\mathrm{Re}\,(a_1)}{\exp\left[-2\,\mathrm{Re}\,(a_1)\,\tau\right] - \mathrm{Re}\,(a_2)}\right]^{\frac{1}{2}}. \tag{29}$$

If the cubic term in (27) is neglected ($A \to 0$), one recovers the usual exponential behaviour of $|A|$ predicted by the linear theory: the amplitude grows when F_d is larger than F_{dc} (this implies positive values of the real part of a_1) and decays when F_d is smaller than F_{dc} (this implies negative values of the real part of a_1). Nonlinear terms have different effects depending on the values of the parameters. In order to discuss the behaviour of $|A|$ let us consider first F_d larger than F_{dc} and consequently positive values of the real part of a_1. If the other parameters are such that the real part of a_2 is negative, nonlinear effects cause the perturbation to reach the equilibrium amplitude $|A_e|$ when τ tends to infinity:

$$|A_e| = \left[-\frac{\mathrm{Re}\,(a_1)}{\mathrm{Re}\,(a_2)}\right]^{\frac{1}{2}}. \tag{30}$$

(Note that the term 'amplitude' is used both for the amplitude of the ripple and for the function $A(\tau)$. Its meaning will be clear from the context.) The value of $|A|$ tends to $|A_e|$ with a monotonic growth or decay depending on its initial value. On the other

hand, if the values of the parameters are such that the real part of a_2 is positive, no equilibrium amplitude exists and the perturbation tends to grow indefinitely.

A different behaviour is present when F_d is smaller than F_{dc}, i.e. for negative values of the real part of a_1. If the values of the other parameters are such that the real part of a_2 is also negative, any perturbation tends to decay. On the other hand, if the real part of a_2 is positive, perturbations characterized by an initial amplitude larger than $|A_e|$ amplify and tend to grow indefinitely. If the initial amplitude is smaller than $|A_e|$, perturbations decay.

The configuration of the bottom under sea waves is thus determined by the values of the parameters which affect the time development of $|A|$. This will be discussed in the following section.

3. Results

As pointed out in the previous section the smallness of the parameter Q allowed us to decouple the study of the oscillatory flow from that concerning the time development of the bottom.

We first discuss the flow field. As already explained in I, the flow field exhibits a complex structure but the time development of the bottom is mainly controlled by its steady part. The steady streaming consists of recirculating cells; their number, shape and intensity depending on the parameters of the problem. The results described in I, which concern the flow over ripples of infinitesimal amplitude, are modified by nonlinear effects as explained in detail in Vittori (1989). We recall here only the main features of the flow field which are relevant to the discussion of present results concerning the bottom time development. When according to linear theory the steady streaming is characterized by the presence of four cells, nonlinear effects cause the upper pair of cells to squeeze in a gap between the lower cells (see figure 1). When only two cells are present nonlinear effects tend to shift the centres of the cells towards the troughs of the ripples (see figure 2). These modifications of the flow affect bottom elevation. In particular they cause a bottom second harmonic to be present, the amplitude of which is such that the component of sediment weight along the bed profile at second order exactly balances the component of the drag force acting on the sediment.

Let us now focus our attention on the development of bedforms. In I a bottom perturbation of infinitesimal amplitude has been considered and the conditions for its growth or decay have been determined. The analysis described in the previous sections allowed us to treat perturbations of small but finite amplitude. Assuming that bottom perturbations of finite amplitude are originated only by the time development of initially infinitesimal perturbations, for fixed values of R_d, the plane (R_δ, F_d) can be divided into three regions where the present theory predicts the existence of a flat bed, rolling-grain ripples and vortex ripples respectively. These three regions are sketched in figure 3 (*a*). Indeed for F_d less than F_{dc}, (27) states that any infinitesimal perturbation tends to decay (flat bed). On the other hand, if F_d is larger than F_{dc}, bottom perturbations characterized by wavenumbers falling within a restricted range around α_c amplify and ripples appear. The initial time development of the amplitude of the latter is always described by (29).

In the region where F_d is less than F_{dv}, $|A_e|$ is such that the ratio k between ripple height and length is less than 0.1. Thus rolling-grain ripples are the bottom configuration predicted by the theory. In this region (29) can be assumed to describe the time development of an initially infinitesimal perturbation till it reaches its final

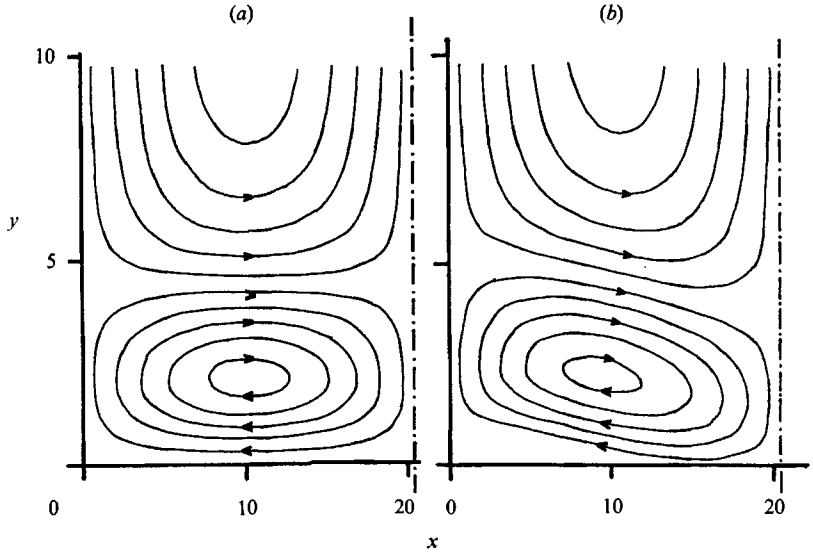

FIGURE 1. Steady part of the stream function, (*a*) neglecting or (*b*) considering nonlinear effects ($\alpha = 0.15$, $R_\delta = 0.1$, $C_{22}^{(0)} = 0$, $\epsilon^{\frac{1}{2}} = 0.3$).

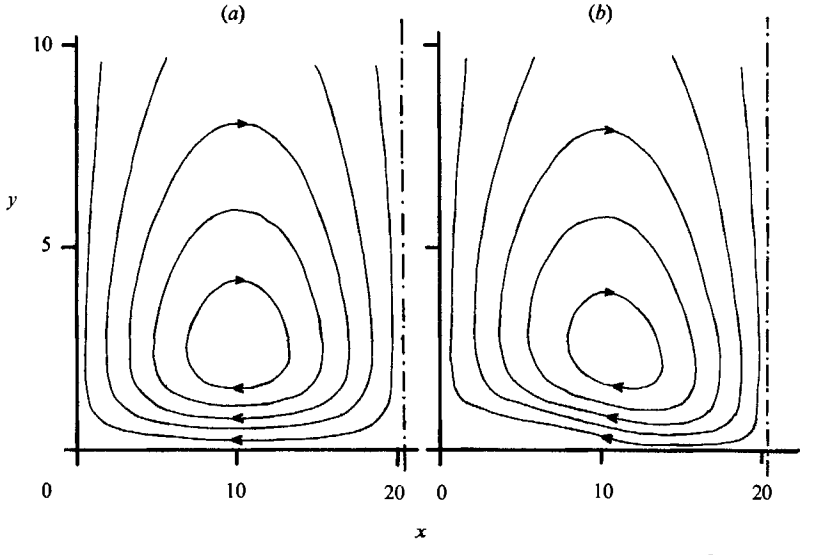

FIGURE 2. Steady part of the stream function, (*a*) neglecting or (*b*) considering nonlinear effects ($\alpha = 0.15$, $R_\delta = 80$, $C_{22}^{(0)} = 0$, $\epsilon^{\frac{1}{2}} = 0.3$).

equilibrium configuration. If F_d is larger than F_{dv}, the value of $|A_e|$ is such that k is larger than 0.1. In this region (29) describes the time development of an initially infinitesimal perturbation only till the flow separates behind the crests. Then the present theory cannot follow the further growth of ripples in the 'vortex regime'. Indeed the assumption of weakly nonlinear effects is such that the strong nonlinear effects associated with flow separation cannot be handled by the present theory. Thus, if F_d is larger than F_{dv}, it can only be concluded that vortex ripples will presumably appear though the time development of their amplitude cannot be predicted. So far it has been assumed that a_2 is negative for any value of R_δ, i.e. it

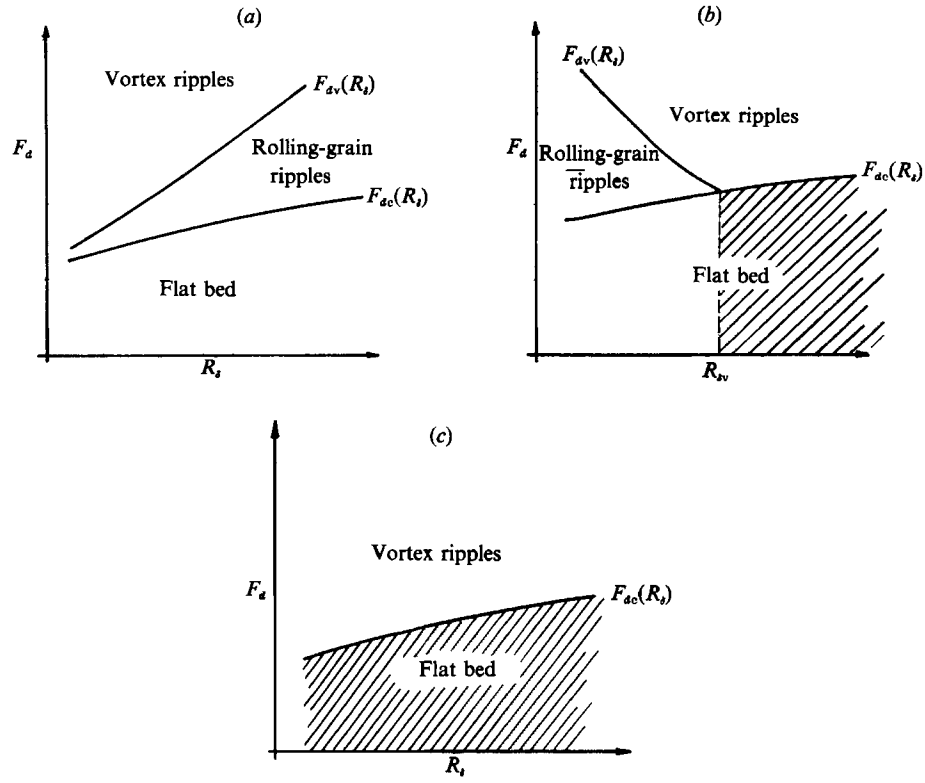

FIGURE 3. Sketches of the limiting curves dividing the (R_δ, F_d)-plane into regions where a flat bed, rolling-grain ripples and vortex ripples are expected to form (fixed values of s and R_d). (*a*) $a_2 < 0$ for any value of R_δ; (*b*) $a_2 < 0$ for $R_\delta < R_{\delta v}$ and $a_2 > 0$ for $R_\delta > R_{\delta v}$; (*c*) $a_2 > 0$ for any value of R_δ.

has a different sign with respect to a_1 when F_d is larger than F_{dc}. The case of a_2 changing sign for R_δ equal to $R_{\delta v}$ is sketched in figure 3(*b*): the real part of a_2 (which is assumed negative for low values of R_δ) increases when R_δ increases and becomes positive for R_δ larger than $R_{\delta v}$. In this case the curve $F_{dv}(R_\delta)$ merges with the curve $F_{dc}(R_\delta)$ and for R_δ larger than $R_{\delta v}$ the region where rolling-grain ripples are the bedforms predicted by the theory disappears (see figure 3*b*). Indeed for R_δ larger than $R_{\delta v}$ and F_d larger than F_{dc}, $|A_e|$ is imaginary, no equilibrium exists and bottom perturbations tend to grow indefinitely.

Finally, if a_2 is positive for any value of R_δ, no region of the (R_δ, F_d)-plane exists where rolling-grain ripples are a stable bed configuration and the instability of the flat bed always leads to a vortex-ripple regime (see figure 3*c*).

An example of the results obtained for R_d equal 10 is shown in figure 4. For this value of R_d increasing R_δ, both F_{dc} and F_{dv} increase. In the same figure experimental points from Blondeaux, Sleath & Vittori (1988) are also shown. The data are the same as in figure 10(*a*) of I and consequently the values of R_d fall in the range (5, 15). However, in figure 4 observed ripples are plotted accordingly to their type: rolling-grain and vortex ripples. The qualitative agreement seems satisfactory though the span of the rolling-grain region is theoretically overestimated. In the region of the plane (R_δ, F_d) where rolling-grain ripples are a stable bed configuration, the present analysis allows the prediction of their geometrical configuration. Indeed relationship (30) gives the equilibrium amplitude of the ripple, where (23) determines the relative

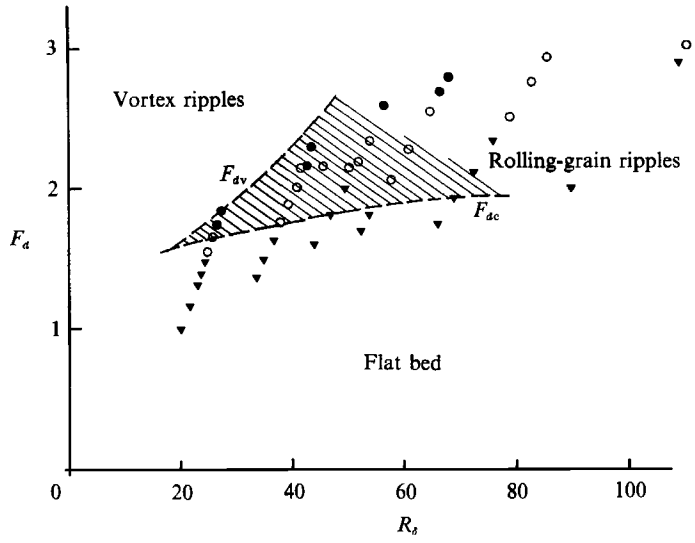

FIGURE 4. Limiting curves dividing the (R_δ, F_d)-plane into regions where a flat bed, rolling-grain ripples and vortex ripples are expected to form ($R_d = 10$, $\beta = 0.15$, $s = 2.65$). Experimental data of Blondeaux *et al.* (1988) are for $5 < R_d < 10$ (▼, flat bed; ○, rolling-grain ripples; ●, vortex ripples).

Exp. no.	R_d	F_d	R_δ	Experimental value of h^*/δ^*	Theoretical value of h^*/δ^*
1	10.4	2.08	57.9	0.90	0.54
3	11.6	2.28	61.0	0.72	0.84
4	13.0	2.57	64.9	0.82	1.14
12	9.7	1.90	39.6	0.50	0.71
13	10.4	2.03	41.0	1.21	1.04
31	8.4	1.67	26.0	1.05	0.56
37	11.2	2.19	52.1	0.64	0.97
38	12.0	2.34	53.9	1.24	1.19

TABLE 1. Experimental data from Blondeaux *et al.* (1988) for sand ($d^* = 0.124$ mm)

amplitude of the second harmonic of the ripples profile with respect to the fundamental.

In table 1 and figure 5 the experimental values of ripple height (h^*) are compared with those predicted by the present theory. The experiments considered in figure 5 correspond to those of figure 4 and are characterized by values of R_d falling in the range (5, 15). The agreement seems satisfactory taking into account that the dashed lines in figure 5 are such that the points falling between them are characterized by a theoretical value which differs from the experimental value by an amount equal to 50 % of the latter. An example of the predicted ripple profile is shown in figure 6. The typical shape with sharper peaks and flatter troughs is clearly recognizable (it is worth pointing out that the vertical coordinate has been magnified by a factor 3). A quantitative comparison between experimental and theoretical ripple profiles is not possible since, to the authors' knowledge, detailed measurements of rolling-grain ripple profiles do not exist.

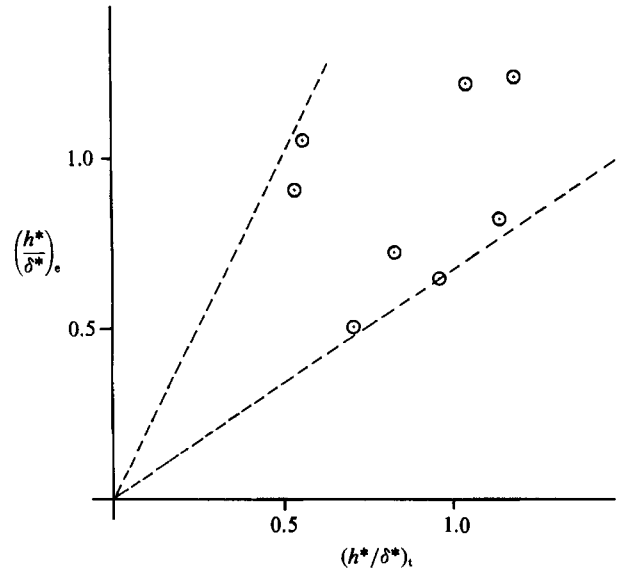

FIGURE 5. Theoretical prediction of ripple height plotted versus experimental values of Blondeaux *et al.* (1988).

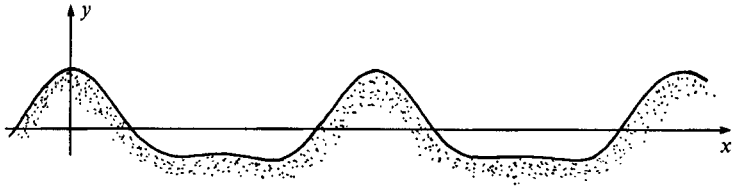

FIGURE 6. Predicted equilibrium bottom configuration ($R_\delta = 40$, $R_d = 10$, $s = 2.65$, $\beta = 0.15$, $F_d = 1.90$).

In the above-mentioned region of the plane (R_δ, F_d), i.e. when rolling-grain ripples are present, knowing their geometrical profile and the flow field which is obtained from the stream function ψ, it is possible to compute some important quantities which control the interaction between surface waves and the sea bottom. In particular the bed shear stress τ^* and the energy dissipation P^*, averaged in time and space, which takes place in the bottom boundary layer are given by

$$P^* = \frac{1}{T^*}\int_0^{T^*}\frac{\alpha^*}{2\pi}\int_0^{\alpha^*/2\pi}\int_{\eta^*(x^*)}^{\infty}\left[4\mu\left(\frac{\partial^2\psi^*}{\partial x^*\,\partial y^*}\right)^2+\mu\left(\frac{\partial^2\psi^*}{\partial y^{*2}}+\frac{\partial^2\psi^*}{\partial x^{*2}}\right)^2\right]\mathrm{d}x^*\,\mathrm{d}y^*\,\mathrm{d}t^*, \quad (31a)$$

$$\tau^* = -\frac{4\mu(\partial\eta^*/\partial x^*)}{1+(\partial\eta^*/\partial x^*)^2}\frac{\partial^2\psi^*}{\partial x^*\,\partial y^*}+\mu\frac{1-(\partial\eta^*/\partial x^*)}{1+(\partial\eta^*/\partial x^*)}\left(\frac{\partial^2\psi^*}{\partial y^{*2}}-\frac{\partial^2\psi^*}{\partial x^{*2}}\right) \quad \text{at} \quad y^* = \eta^*(x^*). \quad (31b)$$

Introducing the dimensionless quantities $P = P^*/\rho U_0^{*3}$, $\tau = \tau^*/\rho U_0^{*2}$ and taking into account that the stream function and the bottom profile are expressed in power series of $\epsilon^{\frac{1}{2}}$ it is easy to see that

$$P = P_0+\epsilon^{\frac{1}{2}}P_1+\epsilon P_2+O(\epsilon^{\frac{3}{2}}), \quad \tau = \tau_0+\epsilon^{\frac{1}{2}}\tau_1+\epsilon\tau_2+O(\epsilon^{\frac{3}{2}}). \quad (32a, b)$$

For the sake of brevity we do not report the expressions for P_0, P_1, P_2 and τ_0, τ_1, τ_2. As

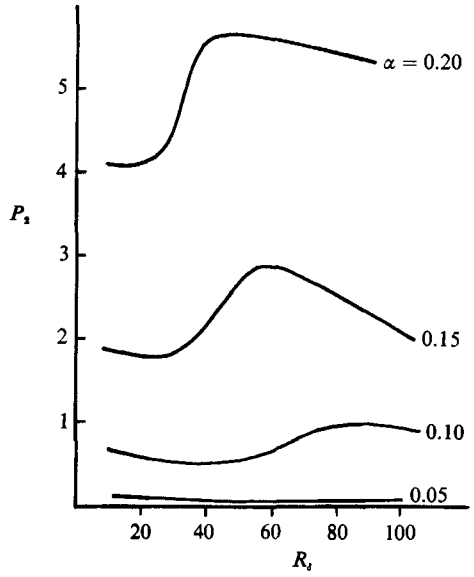

FIGURE 7. Function P_2 plotted versus R_δ for different values of the ripples wavenumber α.

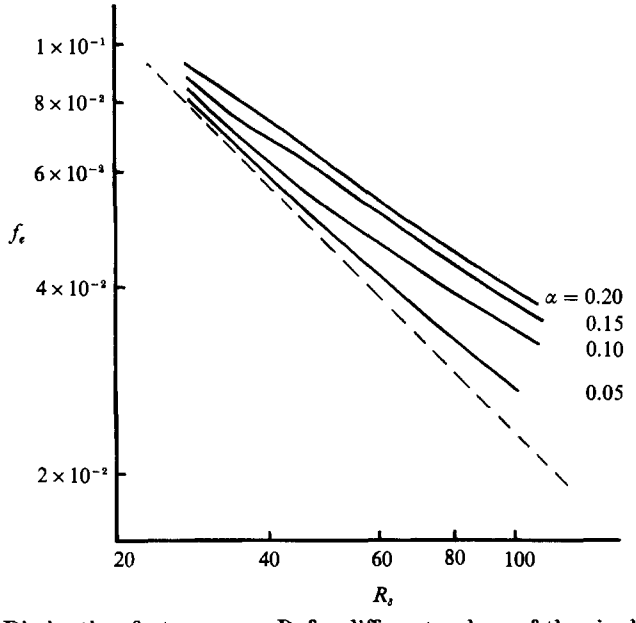

FIGURE 8. Dissipation factor versus R_δ for different values of the ripple wavenumber α and $k = 0.1$.

far as energy dissipation is concerned we only point out that (i) P_0 is the wave energy dissipation per unit time and space for a flat bed; (ii) P_1 identically vanishes. This result is obvious since the wave energy dissipation cannot depend on the sign of ripple amplitude; (iii) the last term P_2 depends on α and R_δ. In figure 7, P_2 is plotted versus R_δ for different values of α. The increase of P_2 found for a fixed value of α as R_δ increases is related to the different structure of the steady drift which is present in the oscillatory flow over a wavy bed. Indeed, for fixed α, a transition occurs as R_δ

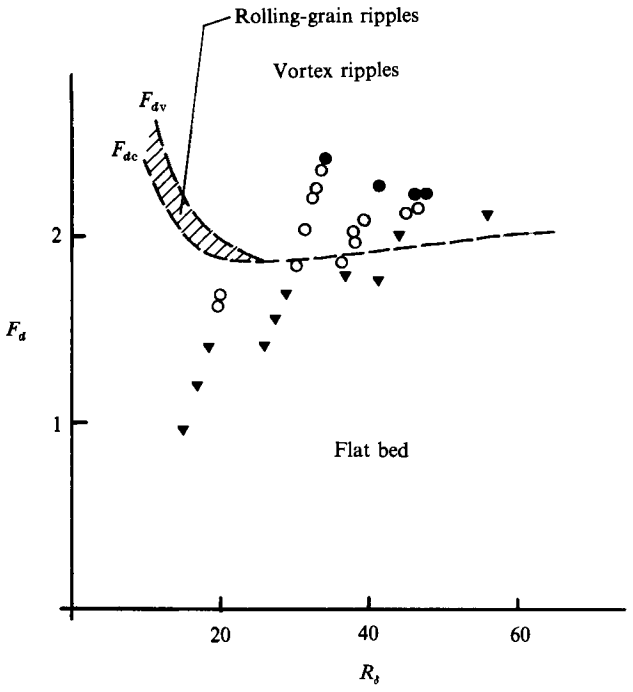

FIGURE 9. Limiting curves dividing the (R_δ, F_d)-plane into regions where a flat bed, rolling-grain ripples and vortex ripples are expected to form ($R_d = 20$, $\beta = 0.15$, $s = 2.65$). Experimental data of Blondeaux *et al.* (1988) are for $15 < R_d < 25$ (▼, flat bed; ○, rolling-grain ripples; ●, vortex ripples).

increases from a regime characterized by steady streaming consisting of four recirculating cells to a two-cell regime (Vittori 1989).

In figure 8 the behaviour of the dissipation factor f_e, defined by Jonsson (1963) as the ratio between P^* and $2\rho U_0^{*3}/3\pi$, is shown as function of R_δ for different values of ripple wavenumber α and assuming a value of the ratio k between ripple height and length equal to 0.1. In this figure the dashed line corresponds to a flat bed. For a fixed value of the ripple steepness k, the increase of P_2 caused by the increase of α is such that the term ϵP_2 increases even though ϵ decreases in order to have a fixed value of k. Consequently short ripples are characterized by larger values of f_e than longer but similar ripples. For R_δ less than about 100 these findings are in agreement with results by Sleath (1984, p. 203), who computed f_e starting from knowledge of the oscillatory flow over a rippled bed determined by means of the numerical integration of the vorticity equation without any assumption on the value of ϵ and r. For R_δ larger than about 100, Sleath's results deviate from the present results since for such values of the parameters the flow separates and vortex shedding occurs. Similar results are obtained for the bed shear stress.

So far we have described a comparison between the theoretical predictions and experimental data when R_d is equal to 10. The agreement between theory and experiments get worse when larger values of R_d are considered. Figure 9 shows the theoretical curves dividing the plane (R_δ, F_d) into the three regions (flat bed; rolling-grain ripples; vortex ripples) for $R_d = 20$ along with experimental data from Blondeaux *et al.* (1988) with R_d falling in the range (15, 25). In this case only a qualitative agreement is found. Indeed either theoretical results or experimental

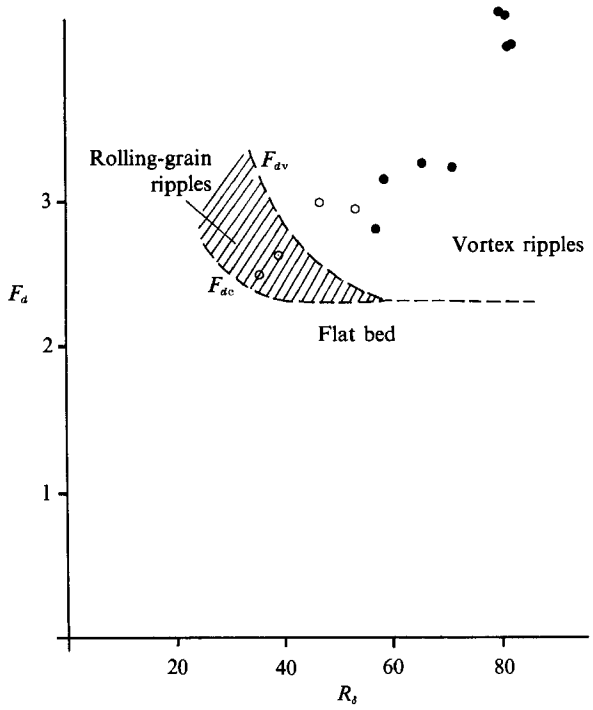

FIGURE 10. Limiting curves dividing the (R_δ, F_d)-plane into regions where a flat bed, rolling-grain ripples and vortex ripples are expected to form ($R_d = 40$, $\beta = 0.15$, $s = 2.65$). Experimental data by Horikawa & Watanabe (1968) are for $30 < R_d < 50$ (▼, flat bed; ○, rolling-grain ripples; ●, vortex ripples).

data show that an increase of R_δ implies a decrease of F_{dv} and consequently a decrease of the area where rolling-grain ripples are a stable bed configuration. Similar results are obtained when comparing the theory with data by Horikawa & Watanabe (1968) which are characterized by an average value of R_d equal to 40 (see figure 10). The lack of a quantitative agreement can be explained by considering that when R_δ is less than R_d, d^* is larger than δ^*, and in this situation the theory can provide only qualitative information. In order to obtain quantitative information for R_δ less than R_d, it would be necessary to extend the theory taking into account the large momentum transfer due to the vorticity shed by sand grains.

There are other experimental data on rolling-grain ripples which have not been considered herein. Indeed all of them are characterized by values of the Stokes Reynolds number R_δ larger than the critical value for laminar–turbulent transition of about 100 (Merkly & Thomann 1975; Tromans 1976; Hino, Sawamoto & Takasa 1976; Blondeaux & Seminara 1979; Blondeaux 1987). In this situation the different structure of the basic flow is likely to significantly affect the development of bedforms.

In describing what happens in the plane (R_δ, F_d) it has been assumed that the initial perturbation has an infinitesimal amplitude. When considering initial perturbations of finite amplitude, the results described so far are slightly modified. Indeed, depending on the values of the parameters, a portion of the region where the theory predicts a flat bed might exist where finite but small-amplitude perturbations grow and lead to the appearance of vortex ripples. This happens only when a_2 is positive, i.e. in the situation sketched in figure 3(*b*) for R_δ larger than $R_{\delta v}$ or for any value of

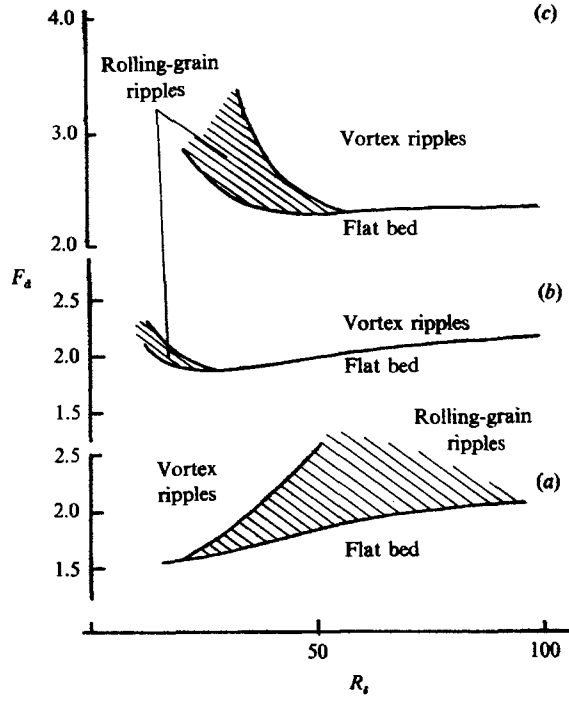

FIGURE 11. Limiting curves dividing the (R_δ, F_d)-plane into regions where a flat bed, rolling-grain ripples and vortex ripples are expected to form. (*a*) $R_d = 10$; (*b*) $R_d = 20$; (*c*) $R_d = 40$ ($\beta = 0.15$, $s = 2.65$).

R_δ in the situation sketched in figure 3 (*c*). Indeed in the dashed region, a vortex ripple might appear if the initial perturbation has an amplitude larger than $2(F_{dc} - F_d)^{\frac{1}{2}}|A_e|$.

We conclude that rolling-grain ripples are an equilibrium configuration only within a restricted region of the plane (R_δ, F_d), provided that the initial amplitude of the bottom perturbation is small. Outside the latter region the plane bottom is either stable or rolling-grain ripples appear as a transient bedform which eventually leads to vortex ripple. This is summarized in figure 11.

4. Discussion

In I and in the present paper the time development of a small perturbation of a cohesionless bottom subject to the action of a gravity wave has been studied in the linear and nonlinear regimes.

We now focus our attention on the assumptions made and consequently on the limitations of the present theory. First, a viscous flow has been assumed, whence the analysis is restricted to sufficiently low values of R_δ. The linear stability analysis of Blondeaux & Seminara (1979) suggests that for flow to remain laminar R_δ must not exceed a value of about 100. However, the latter authors adopted a momentary criterion of instability and the predicted instability is limited to a small part of the cycle. The recent work by Blondeaux & Colombini (1988), where the time development of two-dimensional disturbances of a flat Stokes layer have been studied by means of a direct simulation technique, seems to indicate that perturbations of laminar flow are present for values of the Reynolds number in the

Blondeaux *et al.*								Sleath
Sand: $d^* = 0.4$ mm		Sand: $d^* = 0.2$ mm		Sand: $d^* = 0.124$ mm		Nylon pellets: $d^* = 0.42$ mm		Sand: $d^* = 0.4$ mm
Exp. no.	$h^*/2\delta_1^*$	Exp. no.	$h^*/2\delta_1^*$	Exp. no.	$h^*/2\delta_1^*$	Exp. no.	$h^*/2\delta_1^*$	$h^*/2\delta_1^*$
								0.58
8	0.51	13	0.20	1	0.17	2	0.31	0.50
9	0.46	14	0.21	3	0.18	7	0.25	0.48
10	0.52	20	0.33	4	0.22	11	0.29	0.45
15	0.53	26	0.15	12	0.19	12	0.30	0.83
30	0.35	27	0.20	13	0.19	16	0.32	0.80
31	0.34	28	0.23	21	0.15	17	0.39	0.59
32	0.36	29	0.29	22	0.18	25	0.35	0.48
33	0.41	35	0.68	31	0.18	29	0.27	0.78
35	0.44	36	0.20	32	0.23	39	0.30	0.92
36	0.48	42	0.34	38	0.19	49	0.29	1.11
45	0.46	44	0.28	42	0.25	50	0.26	1.02
46	0.44			44	0.22			0.68
				46	0.18			0.69
				48	0.14			0.61
								1.34
								1.07
								0.88
								0.68
								0.59
								0.62

TABLE 2. Experimental data on the ratio between ripple amplitude and the thickness of the viscous boundary layer, from Blondeaux *et al.* (1988) and Sleath (1976)

range predicted by Blondeaux & Seminara (1979), but their energy remains very low till larger values of R_δ are reached. Experimental data seem to support this conclusion. It can be concluded that the present results can be used with confidence up to values of R_δ around 100, and the theory could also work for larger values of R_δ.

A second limitation derives from the assumption of a smooth wavy bottom. The size of sediment grains should then be much less than the thickness of the viscous boundary layer δ_1^*. For practical purposes the actual value δ_1^* of the boundary-layer thickness can be assumed larger than δ^* and equal to $6.5\nu^{\frac{1}{2}}/\omega^*$ as suggested by Manohar (1955). Comparing the diameter of sand (which ranges between 0.062 mm and 2 mm) with the value of δ_1^* computed using the angular frequency characteristic of sea waves (ω^* can be assumed to be about 0.6 s^{-1}) one can argue that the above assumption is verified under field conditions.

In the present contribution it has also been assumed that nonlinear terms are smaller than other terms in the vorticity equation. This assumption formally implies that the ripple amplitude $\frac{1}{2}h^*$ must be smaller than the thickness of the viscous boundary layer δ^*, i.e. the theory holds for values of ϵ much smaller than one (strictly infinitesimal). However, for practical purposes it could be assumed that the theory provides reasonable results provided that $\frac{1}{2}h^*$ is smaller than δ_1^*. It is easy to verify that the latter quantity is larger than the amplitude of a ripple at incipient separation. In table 2 the values of the ratio $h^*/2\delta_1^*$ are shown for the experiments performed by Blondeaux *et al.* (1988) and Sleath (1976) with medium sand (experimental data by Sleath 1976 referring to nylon pellets and coarse sand are not

shown since for these data d^* is not smaller than the boundary-layer thickness). It can be seen that, except from a few cases, the amplitude of rolling-grain ripples which are about to separate ($h^* = 0.1l^*$) is always smaller than the thickness of the boundary layer.

Finally it must be pointed out that criticism could arise about the sediment flow rate formula proposed in I. It is worth stressing that the critical wavelength α_c, the critical Froude number F_{dc} and the equilibrium amplitude are all not affected by the value attained by the parameter Q but rather by the functional dependence of q on V and $\partial\eta/\partial x$. Comparison of relationship (9) of I with experimental data by Sleath (1978) indicates that the time dependence of q is well predicted even though a discrepancy in the amount of sediment moved by the flow has been detected.

This work has been supported by the Italian Ministry of Education under grant MPI (60%) and is part of G. V.'s Ph.D thesis to be submitted in partial fulfilment of her degree.

Appendix A. Φ_{20}, $\Phi_{22}^{(1)}$ and $\Phi_{22}^{(2)}$

$$\left.\begin{aligned}
&\frac{2}{R_\delta}\frac{\partial^3\Phi_{20}}{\partial t\,\partial^2 y}-\frac{1}{R_\delta}\frac{\partial^4\Phi_{20}}{\partial y^4}=-\mathrm{i}\alpha_c\left[\frac{\partial\bar{\Phi}_1}{\partial y}\left(\frac{\partial^2}{\partial y^2}-\alpha_c^2\right)\Phi_1-\Phi_1\frac{\partial}{\partial y}\left(\frac{\partial^2}{\partial y^2}-\alpha_c^2\right)\bar{\Phi}_1\right]+\text{c.c.},\\
&\frac{\partial\phi_{20}}{\partial y}=-\frac{\partial^2\phi_1}{\partial y^2}-\frac{1}{2}\frac{\partial^3\psi_0}{\partial y^3}+\text{c.c.},\quad y=0,\\
&\frac{\partial\phi_{20}}{\partial y}\to 0\qquad\qquad y\to\infty;
\end{aligned}\right\}\tag{A 1}$$

$$\left.\begin{aligned}
&\frac{2}{R_\delta}\frac{\partial}{\partial t}\left(\frac{\partial^2}{\partial y^2}-4\alpha_c^2\right)\Phi_{22}^{(1)}+2\mathrm{i}\alpha_c\left[\frac{\partial\psi_0}{\partial y}\left(\frac{\partial^2}{\partial y^2}-4\alpha_c^2\right)\Phi_{22}^{(1)}-\Phi_{22}^{(1)}\frac{\partial^3\psi_0}{\partial y^3}\right]\\
&\qquad-\frac{1}{R_\delta}\left(\frac{\partial^2}{\partial y^2}-4\alpha_c^2\right)^2\Phi_{22}^{(1)}\\
&\qquad=-\mathrm{i}\alpha_c\left[\frac{\partial\Phi_1}{\partial y}\left(\frac{\partial^2}{\partial y^2}-\alpha_c^2\right)\Phi_1-\Phi_1\frac{\partial}{\partial y}\left(\frac{\partial^2}{\partial y^2}-\alpha_c^2\right)\Phi_1\right],\\
&\frac{\partial\phi_{22}^{(1)}}{\partial y}=-\frac{\partial^2\phi_1}{\partial y^2}-\frac{1}{2}\frac{\partial^3\psi_0}{\partial y^3},\quad \phi_{22}^{(1)}=-\frac{1}{2}\frac{\partial\phi_1}{\partial y},\quad y=0,\\
&\frac{\partial\phi_{22}^{(1)}}{\partial y}\to 0,\quad \phi_{22}^{(1)}\to 0,\qquad\qquad y\to\infty;
\end{aligned}\right\}\tag{A 2}$$

$$\left.\begin{aligned}
&\frac{2}{R_\delta}\frac{\partial}{\partial t}\left(\frac{\partial^2}{\partial y^2}-4\alpha_c^2\right)\Phi_{22}^{(2)}+2\mathrm{i}\alpha_c\left[\frac{\partial\psi_0}{\partial y}\left(\frac{\partial^2}{\partial y^2}-4\alpha_c^2\right)\Phi_{22}^{(2)}-\Phi_{22}^{(2)}\frac{\partial^3\psi_0}{\partial y^3}\right]\\
&\qquad-\frac{1}{R_\delta}\left(\frac{\partial^2}{\partial y^2}-4\alpha_c^2\right)^2\Phi_{22}^{(2)}=0,\\
&\frac{\partial\phi_{22}^{(2)}}{\partial y}=-\frac{\partial^2\psi_0}{\partial y^2},\quad \phi_{22}^{(2)}=0,\quad y=0,\\
&\frac{\partial\phi_{22}^{(2)}}{\partial y}\to 0,\quad \phi_{22}^{(2)}\to 0,\qquad y\to\infty.
\end{aligned}\right\}\tag{A 3}$$

Appendix B. The functions $f(t)$ and $g(t)$ of (22)

$$f(t) = b\left|2\frac{\partial\psi_0}{\partial y}\right|^{b-1}\left[\mathrm{L}_1\left(\frac{\partial\psi_0}{\partial y}\right)+2\mathrm{L}_1(\Phi_1)+2\frac{\partial\Phi_{22}^{(1)}}{\partial y}\right]$$
$$+\tfrac{1}{2}b(b-1)\left|2\frac{\partial\psi_0}{\partial y}\right|^{b-2}\mathrm{sgn}\left(2\frac{\partial\psi_0}{\partial y}\right)\left[2\left(\frac{\partial^2\psi_0}{\partial y^2}+\frac{\partial\Phi_1}{\partial y}\right)-\mathrm{i}\alpha_c\frac{\beta R_d}{F_{dc}^2}\right]^2 \quad \text{at} \quad y=\frac{R_d}{2R_\delta}, \tag{B 1}$$

$$g(t) = b\left|2\frac{\partial\psi_0}{\partial y}\right|^{b-1}\left[2\left(\frac{\partial^2\psi_0}{\partial y^2}+\frac{\partial\Phi_{22}^{(2)}}{\partial y}\right)-2\mathrm{i}\alpha_c\frac{\beta R_d}{F_{dc}^2}\right] \quad \text{at} \quad y=\frac{R_d}{2R_\delta}, \tag{B 2}$$

where
$$\mathrm{L}_1 \equiv \frac{\partial^2}{\partial y^2}+\alpha_c^2. \tag{B 3}$$

Appendix C. The functions $h(t)$ and $l(t)$ of (26)

$$h(t) = b\left|2\frac{\partial\psi_0}{\partial y}\right|^{b-1}\left[2\left(\frac{\partial^2\psi_0}{\partial y^2}+\frac{\partial\Phi_1}{\partial y}\right)-\mathrm{i}\alpha_c\frac{\beta R_d}{F_{dc}^2}\right] \quad \text{at} \quad y=\frac{R_d}{2R_\delta} \tag{C 1}$$

$$l(t) = 2b\left|2\frac{\partial\psi_0}{\partial y}\right|^{b-1}\left\{\frac{\partial\Phi_{31}^{(1)}}{\partial y}+\frac{\partial^2\Phi_{20}}{\partial y^2}+\mathrm{L}_2\left(\Phi_{22}+C_{22}^0\left(\bar{\Phi}_1+\frac{\partial\psi_0}{\partial y}\right)\right)\right.$$
$$\left.+\tfrac{1}{2}\mathrm{L}_3\left(\frac{\partial^2\psi_0}{\partial y^2}+\frac{\partial\bar{\Phi}_1}{\partial y}+2\frac{\partial\Phi_1}{\partial y}\right)\right\}+2b(b-1)\left|2\frac{\partial\psi_0}{\partial y}\right|^{b-2}\mathrm{sgn}\left(2\frac{\partial\psi_0}{\partial y}\right)$$
$$\left\{\left[2\left(\frac{\partial\Phi_1}{\partial y}+\frac{\partial^2\psi_0}{\partial y^2}\right)-\mathrm{i}\alpha_c\frac{\beta R_d}{F_{dc}^2}\right]\left[\frac{\partial\Phi_{20}}{\partial y}+\mathrm{L}_3\left(\frac{\partial\psi_0}{\partial y}+\Phi_1+\bar{\Phi}_1\right)\right]\right.$$
$$+\left[2\left(\frac{\partial\bar{\Phi}_1}{\partial y}+\frac{\partial^2\psi_0}{\partial y^2}\right)+\mathrm{i}\alpha_c\frac{\beta R_d}{F_{dc}^2}\right]\left[\frac{\partial\Phi_{22}}{\partial y}+\mathrm{L}_1\left(\frac{1}{2}\frac{\partial\psi_0}{\partial y}+\Phi_1\right)\right.$$
$$\left.\left.+C_{22}^0\left(\frac{\partial^2\psi_0}{\partial y^2}+\mathrm{i}\alpha_c\frac{\beta R_d}{F_{dc}^2}\right)\right]\right\}+\tfrac{1}{2}b(b-1)(b-2)\left|2\frac{\partial\psi_0}{\partial y}\right|^{b-3}$$
$$\left\{\left[2\left(\frac{\partial\bar{\Phi}_1}{\partial y}+\frac{\partial^2\psi_0}{\partial y^2}\right)+\mathrm{i}\alpha_c\frac{\beta R_d}{F_{dc}^2}\right]\left[2\left(\frac{\partial\Phi_1}{\partial y}+\frac{\partial^2\psi_0}{\partial y^2}\right)-\mathrm{i}\alpha_c\frac{\beta R_d}{F_{dc}^2}\right]^2\right\} \quad \text{at} \quad y=\frac{R_d}{2R_\delta}, \tag{C 2}$$

where
$$\mathrm{L}_2 \equiv \frac{\partial^2}{\partial y^2}-2\alpha_c^2; \quad \mathrm{L}_3 \equiv \frac{\partial^2}{\partial y^2}-\alpha_c^2; \quad \Phi_{22} \equiv \Phi_{22}^{(1)}+C_{22}^{(0)}\Phi_{22}^{(2)}. \tag{C 3}$$

REFERENCES

Blondeaux, P. 1987 Turbulent boundary layer of the bottom of gravity waves. *J. Hydraul. Res.* **25**, 447–464.

Blondeaux, P. 1990 Sand ripples under sea waves. Part 1. Ripple formation. *J. Fluid Mech.* **218**, 1–17, (referred to herein as I).

Blondeaux, P. & Colombini, M. 1988 Two-dimensional vortical structures in transitional unsteady boundary layers. *Euromech 235, Patras, May–June.*

Blondeaux, P. & Seminara, G. 1979 Transizione incipiente al fondo di un'onda di gravita. *Rendiconte Accad. Naz. Lincei* **67**, 407–417.

Blondeaux, P., Sleath, J. F. A. & Vittori, G. 1988 Experimental data on sand ripples in an oscillatory flow. *Rep.* 01/88. *Inst. Hydraulics, University of Genoa.*

HINO, M., SAWAMOTO, M. & TAKASU, S. 1976 Experiments on transition to turbulence in an oscillatory pipe flow. *J. Fluid Mech.* **75**, 193–207.

HORIKAWA, K. & WATANABE, A. 1968 Laboratory study on oscillatory boundary layer flow. *Coastal Engng Japan* **11**, 13–28.

JONSSON, I. G. 1963 Measurements in the turbulent wave boundary layer. *Proc. 10th Congr. Intl Assoc. Hydraul. Res., London*, vol. 1, pp. 85–92.

MANOHAR, M. 1955 Mechanics of bottom sediment movement due to wave action. *US Army, Beach Erosion Board Tech. Memo* 75.

MERKLY, P. & THOMANN, H. 1975 Transition to turbulence in oscillatory pipe flow. *J. Fluid Mech.* **68**, 567–575.

SLEATH, J. F. A. 1976 On rolling-grain ripples. *J. Hydraul. Res.* **14**, 69–81.

SLEATH, J. F. A. 1978 Measurements of bed load in oscillatory flow. *J. Waterway Port Coastal Ocean Engng Div.* ASCE **104** (WW3), 291–307.

SLEATH, J. F. A. 1984 *Sea Bed Mechanics.* Wiley.

STUART, J. T. 1971 Non linear stability theory. *Ann. Rev. Fluid Mech.* **3**, 347–370.

TROMANS, P. 1976 The stability of oscillating pipe flow. Abstract of lecture given at *Euromech 73*: *Oscillatory Flows in Ducts, Aix-en-Provence, April 13–15.*

VITTORI, G. 1989 Non-linear viscous oscillatory flow over a small amplitude wavy wall. *J. Hydraul. Res.* **27**, 267–280.

VITTORI, G. 1990 Formation and non-linear development of ripples at the bottom of gravity waves. Ph.D thesis, Genoa University (in Italian).